Electronic Supplemental Document

Caitlin M. Crawford

September 28, 2018

1 PXRD of Quaternary

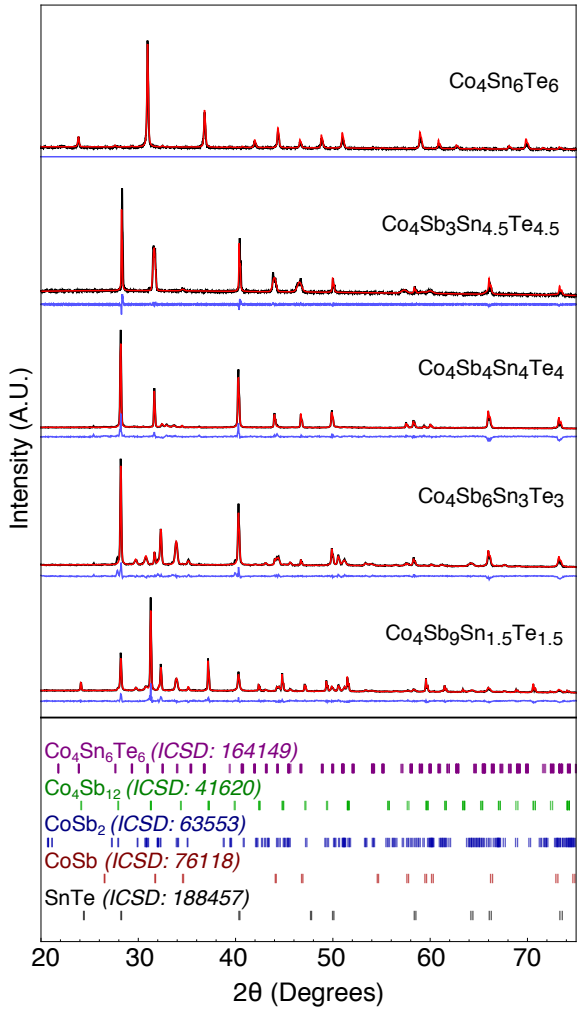

Figure 1: Powder X-ray Diffraction Data: Data of samples 1-4 labeled in Fig. 2. Compositions lie along the pseudo-binary between Co_4Sb_{12} - $Co_4Sn_6Te_6$ in the Co - Sb - $(SnTe)_{0.5}$ phase space. As highlighted in Fig. 2, the XRD breaks up into corresponding triangles that allow us to define our phase space. Experimental (solid black lines), fit profile via TOPAS (solid red lines), and the difference profiles (solid blue lines) are shown for each s ample. Reference patterns are shown below by stick plots with data taken from the ICSD.

2 SEM Photo of Samples

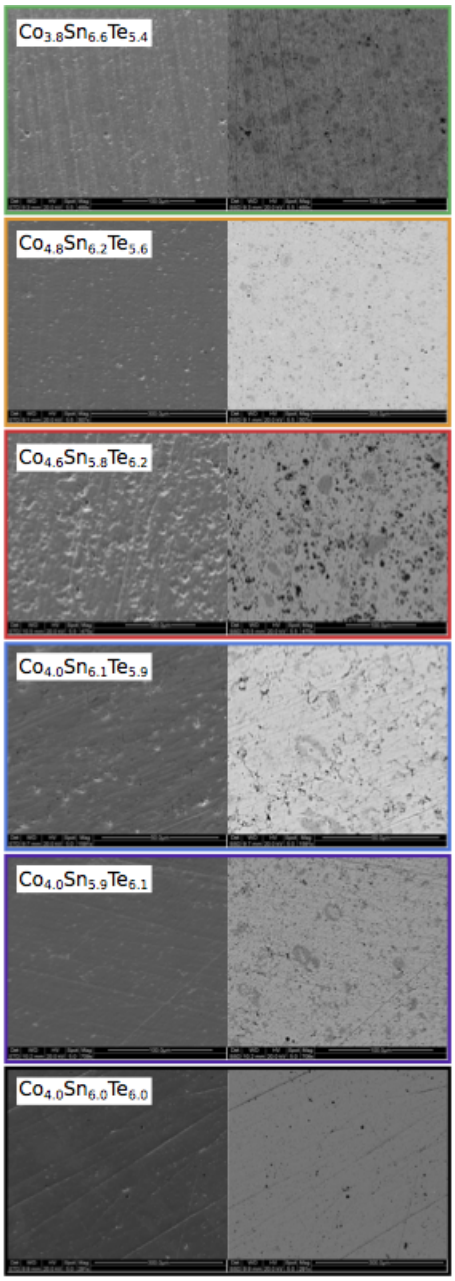

Figure 2: SEM images of samples from produced surrounding the single phase $Co_4Sn_6Te_6$ skutterudite. X-ray diffraction data for these samples can be seem in Fig. 4. Samples were intentionally made with impurity phases following the approach of phase boundary mapping.

3 PXRD Refinement Values for Quaternary

Table 1: TOPAS Refinement Values for Quaternary System

Sample ID	Nominal Composition	Phase One	Phase Two	Phase Three
1	$Co_4Sb_3Sn_{4.5}Te_{4.5}$	SnTe = 36.36%	CoSb = 63.64%	—
2	$Co_4Sb_4Sn_4Te_4$	SnTe = 53.76%	CoSb = 30.13%	$CoSb_2$ = 16.11%
3	$Co_4Sb_6Sn_3Te_3$	SnTe = 38.64%	$CoSb_2$ = 54.22%	CoSb = 7.14%
4	$Co_4Sb_9Sn_{1.5}Te_{1.5}$	SnTe = 18.11%	$CoSb_3$ = 48.34%	$CoSb_2$ = 33.56%
5	$Co_4Sn_6Te_6$	SKD_T = 100%	—	—

Phase fractions found from Rietveld refinement using the TOPAS software package.

Table 2: TOPAS Refinement Values for Quaternary System

Sample ID	R_{wp}	gof
1	10.57	1.520
2	7.475	2.292
3	7.676	2.242
4	6.364	1.943
5	11.564	1.165

Goodness of fit parameters found from Rietveld refinement using the TOPAS software package.

4 DFT Phase Stability Phase Diagram of Quaternary

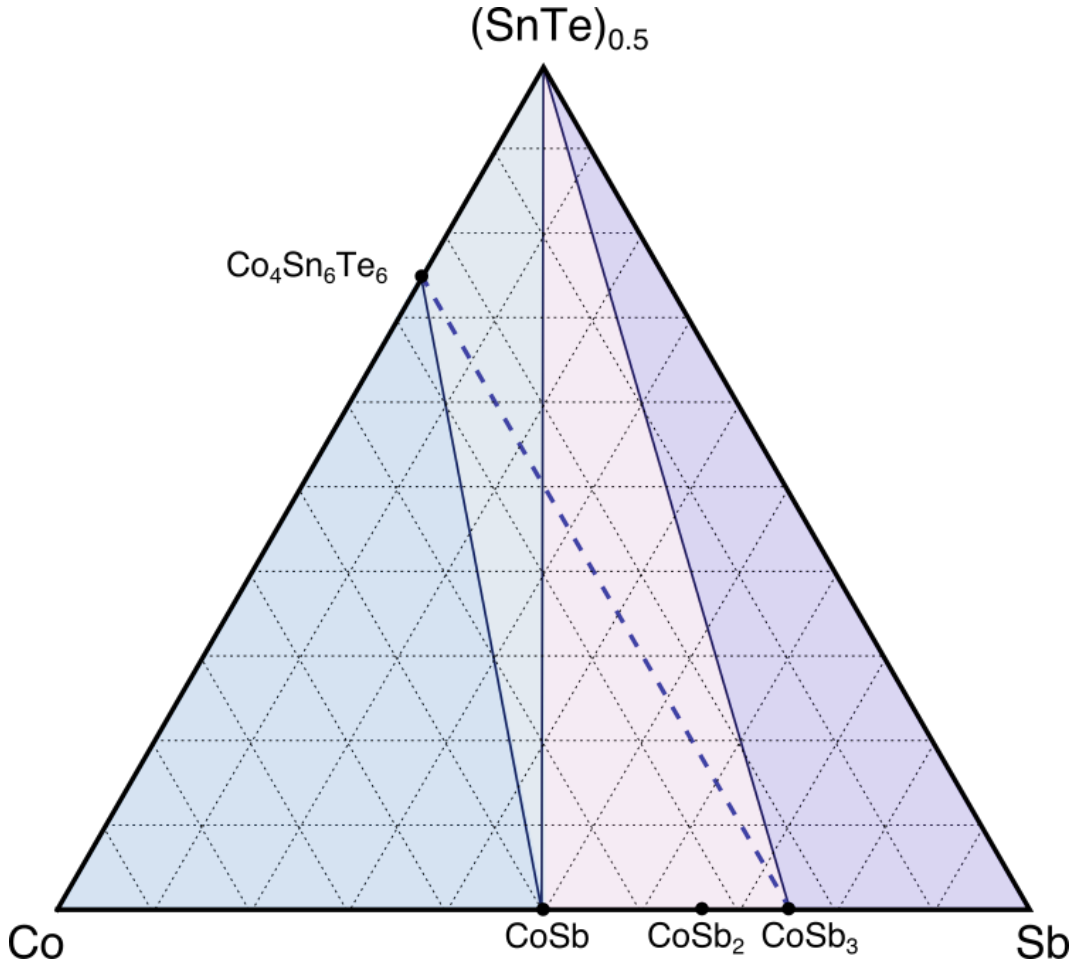

Figure 3: Phase stability analysis of Co-Sb-Sn-Te quaternary system. Theory varies from experiment (Fig. 2) as $CoSb_2$ is not considered an energetically favorable phase. Regardless, no quaternary phase is observed.

5 Argonne's 11-BM Data

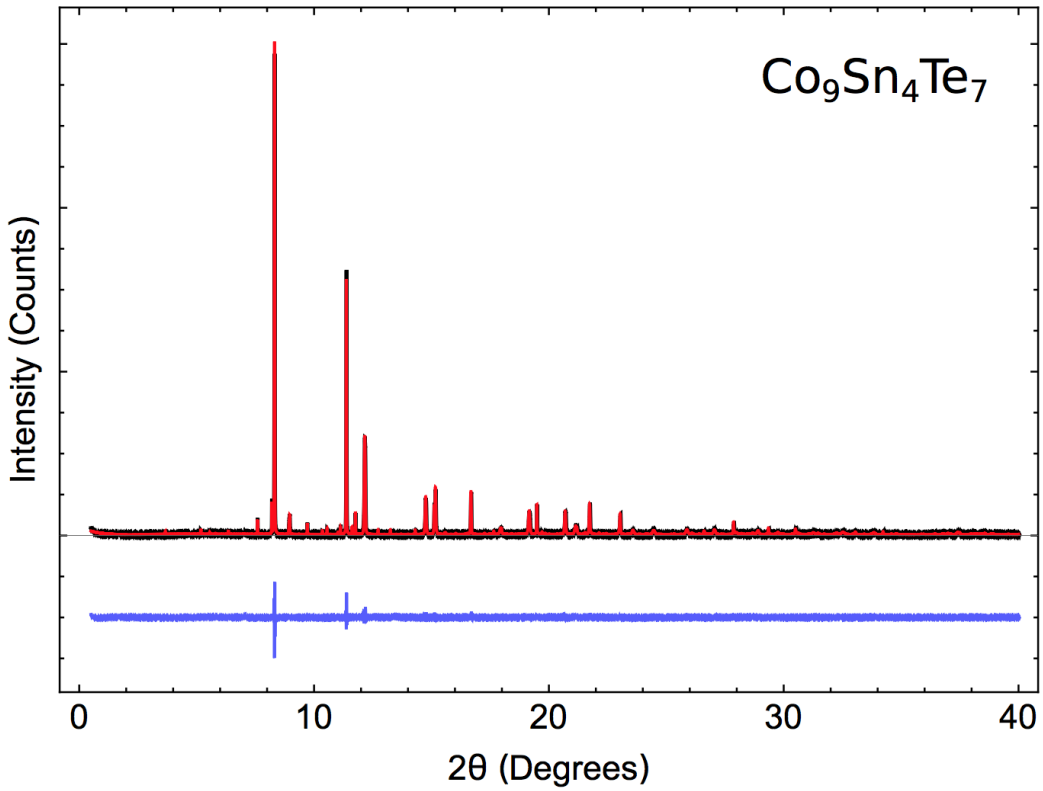

Figure 4: Synchrotron diffraction data of sample with nominal composition $Co_9Sn_4Te_7$ as seen by the blue marker in Fig. 3. Data was refined via TOPAS from ICSD patterns 55564 (CoSn), 164149 ($Co_4Sn_6Te_6$), and 44736 ($Co_{1.67}Te_2$). Diffraction analysis supports the Alkemade lines established in Fig. 3.

6 PXRD Refinement Values for Ternary

Table 3

Nominal Composition	Phase One	Phase Two	Phase Three
$Co_2Sn_3Te_{15}$	SnTe = 26.61%	$CoTe_2$ = 25.02%	Te = 48.36%
$Co_2Sn_3Te_5$	$Co_{1.67}Te_2$ = 14.14%	SnTe = 48.42%	$CoTe_2$ = 37.04%
$CoSn_6Te_3$	SnTe = 77.86%	$CoSn_2$ = 5.00%	$CoSn_3$ = 17.14%
$Co_7Sn_3Te_5$	SKD_T = 26.79%	$Co_{1.67}Te_2$ = 73.21%	—
$Co_9Sn_6Te_5$	SKD_T = 49.50 %	$Co_{1.67}Te_2$ = 35.26%	CoSn = 15.24%
$Co_7Sn_6Te_7$	SKD_T = 67.72 %	$Co_{1.67}Te_2$ = 32.28%	—
$Co_9Sn_4Te_7$	SKD_T = 23.11 %	$Co_{1.67}Te_2$ = 76.89%	—
$Co_9Sn_2Te_4$	$Co_{1.67}Te_2$ = 97.05%	CoSn = 2.95%	—
$CoSn_{1.45}Te_{1.55}$	SKD_T = 66.61 %	SnTe = 18.18 %	$Co_{1.67}Te_2$ = 15.21%
$CoSn_{1.55}Te_{1.45}$	SKD_T = 97.61 %	SnTe = 2.39 %	—
$Co_{0.85}Sn_{1.5}Te_{1.5}$	SKD_T = 73.16 %	SnTe = 23.35 %	$Co_{1.67}Te_2$ = 3.49%
$Co_{2.3}Sn_{5.4}Te_{2.3}$	SnTe = 64.51 %	$CoSn_2$ = 19.39 %	CoSn = 16.10 %
CoTe	CoTe = 100 %	—	—
$Co_{0.8}Te$	$Co_{1.67}Te_2$ = 100%	—	—
$Co_{1.1}Sn_{1.6}Te_{1.4}$	SKD_T = 95.67 %	SnTe = 0.10%	CoSn = 4.23%
$Co_{0.9}Sn_{1.6}Te_{1.4}$	SKD_T = 90.81 %	SnTe = 2.88%	CoSn = 6.31%
$Co_4Sn_{5.99}Te_{6.01}$	SKD_T = 89.40 %	$Co_{1.67}Te_2$ = 4.46%	SnTe = 6.14%
$Co_4Sn_{5.95}Te_{6.05}$	SKD_T = 87.93 %	$Co_{1.67}Te_2$ = 7.43%	SnTe = 4.64%

Phase fractions found from Rietveld refinement using the TOPAS software package for samples in Fig. 3.

Table 4

Nominal Composition	R_{wp}	gof
$Co_2Sn_3Te_{15}$	12.528	1.8695
$Co_2Sn_3Te_5$	14.244	0.3442
$CoSn_6Te_3$	14.089	1.6916
$Co_7Sn_3Te_5$	4.875	1.2448
$Co_9Sn_6Te_5$	5.126	1.143
$Co_7Sn_6Te_7$	3.971	1.266
$Co_9Sn_4Te_7$	10.522	2.239
$Co_9Sn_2Te_4$	4.745	1.236
$CoSn_{1.45}Te_{1.55}$	6.088	1.461
$CoSn_{1.55}Te_{1.45}$	6.85	1.5709
$Co_{0.85}Sn_{1.5}Te_{1.5}$	18.057	1.138
$Co_{2.3}Sn_{5.4}Te_{2.3}$	19.15	1.24
CoTe	11.201	1.034
$Co_{0.8}Te$	15.636	1.333
$Co_{1.1}Sn_{1.6}Te_{1.4}$	8.793	1.2775
$Co_{0.9}Sn_{1.6}Te_{1.4}$	12.628	2.024
$Co_4Sn_{5.99}Te_{6.01}$	12.218	1.085
$Co_4Sn_{5.95}Te_{6.05}$	14.123	1.132

Goodness of fit parameters found from Rietveld refinement using the TOPAS software package. Sample compositions are labeled in the ternary diagram in Figure 3.

Table 5

Nominal Composition	Phase One	Phase Two	Phase Three
$Co_4Sn_6Te_6$	SKD_T = 100%	—	—
$Co_4Sn_{5.9}Te_{6.1}$	SKD_T = 79.15%	$Co_{1.67}Te_2$ = 10.03%	SnTe = 10.82%
$Co_4Sn_{6.1}Te_{5.9}$	SKD_T = 96.27%	SnTe = 3.73%	—
$Co_{4.8}Sn_{6.2}Te_{5.6}$	SKD_T = 64.74%	CoSn = 11.90%	$Co_{1.67}Te_2$ = 23.36%
$Co_{3.8}Sn_{6.6}Te_{5.4}$	SKD_T = 64.92%	CoSn = 11.63 %	SnTe = 23.44%
$Co_{4.6}Sn_{5.8}Te_{6.2}$	SKD_T = 93.16%	$Co_{1.67}Te_2$ = 6.84%	—

Phase fractions found from Rietveld refinement using the TOPAS software package. Samples correspond to Fig. 3's inset.

Table 6

Nominal Composition	R_{wp}	gof
$Co_4Sn_6Te_6$	11.56	1.165
$Co_4Sn_{5.9}Te_{6.1}$	6.654	1.411
$Co_4Sn_{6.1}Te_{5.9}$	6.796	1.540
$Co_{4.8}Sn_{6.2}Te_{5.6}$	20.61	3.057
$Co_{3.8}Sn_{6.6}Te_{5.4}$	10.93	1.448
$Co_{4.6}Sn_{5.8}Te_{6.2}$	5.996	1.161

Goodness of fit parameters found from Rietveld refinement using the TOPAS software package. Sample compositions are labeled in the ternary diagram in Figure 3's inset.

7 Chemical Potential Coordinates

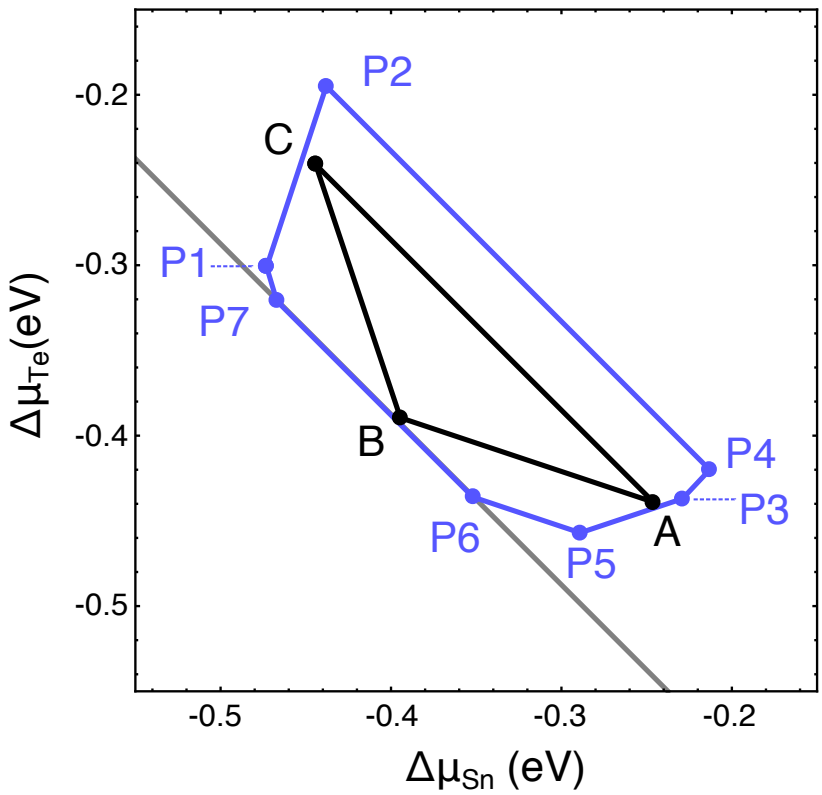

Figure 5: Visual representation of the chemical potential coordinates from the phase stability analysis. The values for the chemical potential coordinates found from the ΔH values below in ES8. Coordinates from the values adjusted (ES8) are shown in black, labeled as A,B, and C. Pre-adjustment coordinates are shown in blue.

Table 7: Chemical Potential Coordinates for Co-Sn-Te System

Point Label	$\Delta\mu_{Co}$ (eV)	$\Delta\mu_{Sn}$ (eV)	$\Delta\mu_{Te}$ (eV)
A	-0.154	-0.246	-0.439
B	-0.0055	-0.3945	-0.3895
C	-0.154	-0.44	-0.241
P1	-0.020	-0.473	-0.301
P2	-0.232	-0.438	-0.195
P3	-0.183	-0.229	-0.437
P4	-0.232	-0.213	-0.420
P5	-0.063	-0.289	-0.457
P6	0.000	-0.352	-0.436
P7	0.000	-0.467	-0.321

Individual coordinates in chemical potential space for the phase stability analysis in the Co-Sn-Te system. A visual representation of the coordinates can be found above.

8 Values of ΔH for each phase in Ternary (pre- and post-adjustment)

Table 8: ΔH values for Ternary System Before Adjustments made Experimental Findings

Stoichiometric Formula			μ	**ΔH (eV)**	**ΔH (eV/atom)**
Co	Sn	Te			
1	0	0	-4.425	-	-
0	1	0	-3.815	-	-
0	0	1	-3.274	-	-
4	6	6	-4.060	-4.726	-0.295
1	1	0	-4.296	-0.352	-0.176
1	2	0	-4.232	-0.641	-0.176
1	3	0	-4.185	-0.870	-0.217
1	0	1	-4.010	-0.321	-0.161
1	0	2	-3.865	-0.622	-0.207
0	1	1	-3.861	-0.633	-0.317
2	1	0	-4.085	0.410	0.137

Pre- Adjustment ΔH values found via computational phase stability analysis. All values were found using the computational methods in Section 2.2.

Table 9: Adjusted ΔH values for Ternary System

	ΔH (eV)			
	Original	Adjusted	Difference (eV)	Difference per atom (eV/atom)
CoTe	-0.321	-0.395	-0.074	-0.037
SnTe	-0.633	-0.685	-0.052	-0.026
CoSn	-0.352	-0.400	-0.048	-0.024

Post- Adjustment ΔH values. The following compounds had their ΔH values adjusted to match the experimental phase diagram. The adjusted valued were used for Figures 7-10. A visual representation of the adjusted phase stability can be found above in ES7.

9 $\Delta H_{D,q}$ for each defect in Ternary

Table 10: $\Delta H_{D,q}$ values for Defects in Co-Sn-Te System

Defect Species	**q**	$\Delta H_{D,q}$(VBM)
$Sn_{Te(1)}$	-2	0.992
$Sn_{Te(1)}$	0	0.874
$Sn_{Te(2)}$	-2	0.975
$Sn_{Te(2)}$	0	0.865
$Te_{Sn(1)}$	0	1.120
$Te_{Sn(1)}$	1	0.891
$Te_{Sn(1)}$	2	0.763
$Te_{Sn(1)}$	0	1.108
$Te_{Sn(1)}$	1	0.882
$Te_{Sn(1)}$	2	0.763
$V_{Te(1)}$	-1	2.645
$V_{Te(1)}$	0	2.339
$V_{Te(2)}$	-2	2.942
$V_{Te(2)}$	-1	2.585
$V_{Te(2)}$	0	2.506
$V_{Sn(1)}$	-2	1.933
$V_{Sn(2)}$	-2	1.918
$V_{Co(1)}$	-2	2.347
$V_{Co(1)}$	-1	2.095
$V_{Co(1)}$	0	2.063
$V_{Co(2)}$	-3	2.637
$V_{Co(2)}$	-1	1.905
$V_{Co(2)}$	0	1.794
Co_i	0	0.920
Co_i	1	0.665
Te_i	-2	1.406
Sn_i	-2	1.900
Sn_i	0	1.331
Sn_i	2	0.894

Enthalpy of formation ($\Delta H_{D,q}$) and charge state (q) for each of the defects considered in Fig. 8. All values were found via computational methods in Section 2.2.

10 Carrier Concentration Heat Map

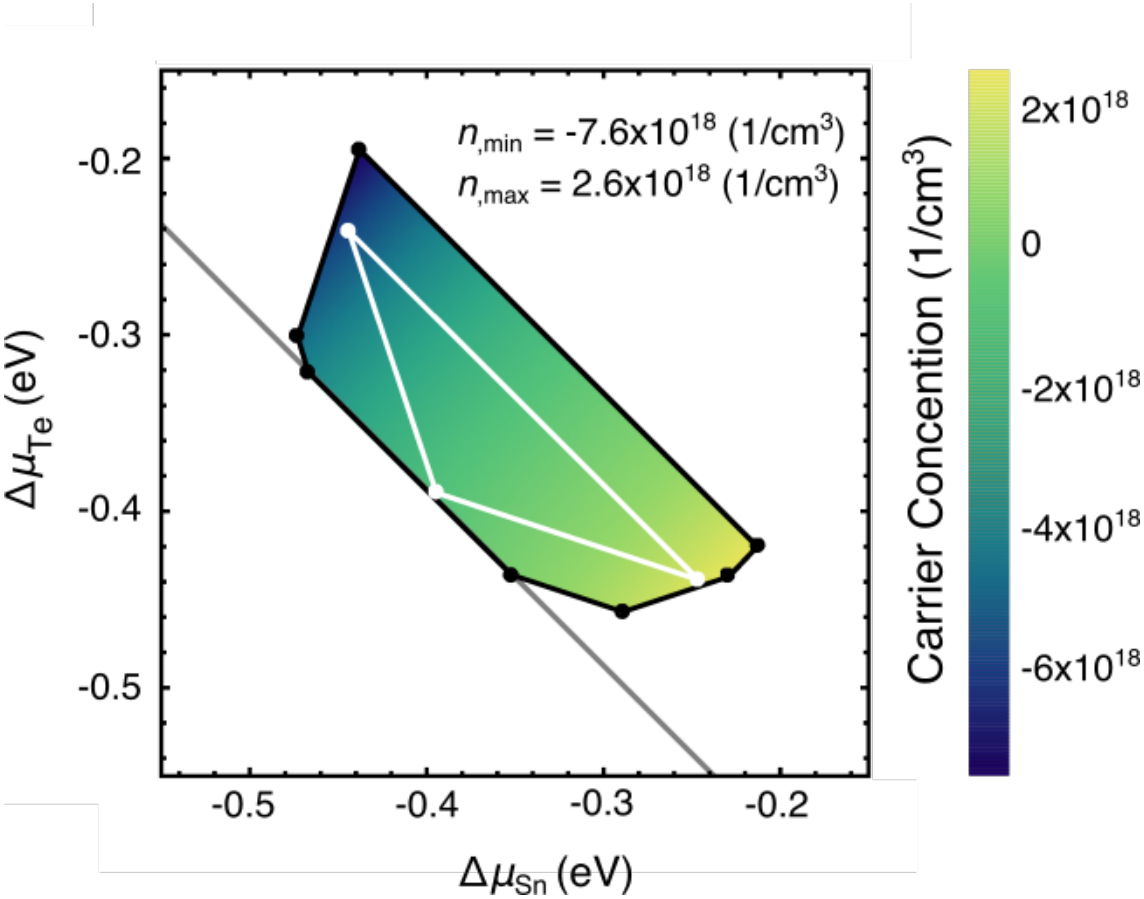

Figure 6: Calculated carrier concentration (using Boltzmann statistics) for pre-adjusted chemical potential coordinates. Adjusted shape is seen overlaid in white.

11 Dopability windows Before Adjustments

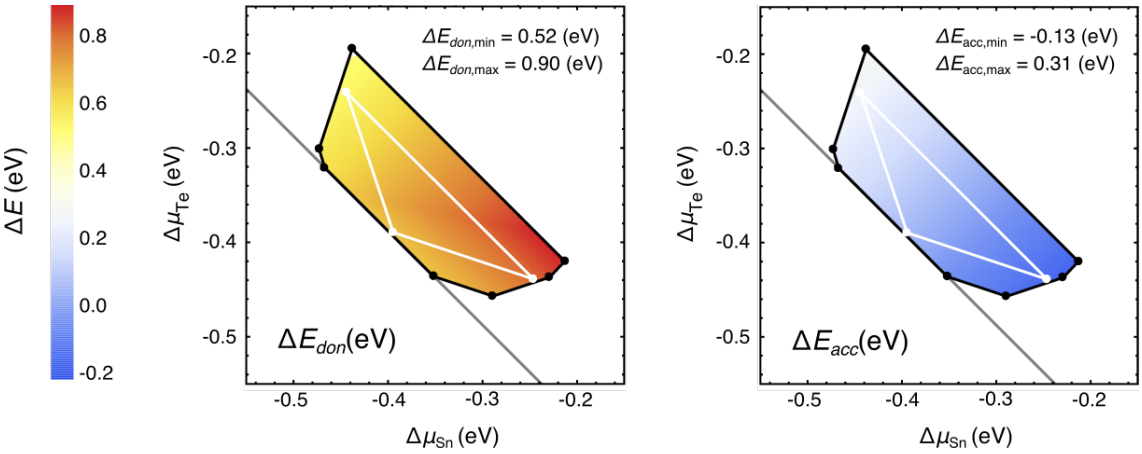

Figure 7: Calculated Dopability windows for pre-adjusted chemical potential coordinates. Adjusted shape is seen overlaid in white.

12 Equilibrium Fermi Energy Before Adjustment

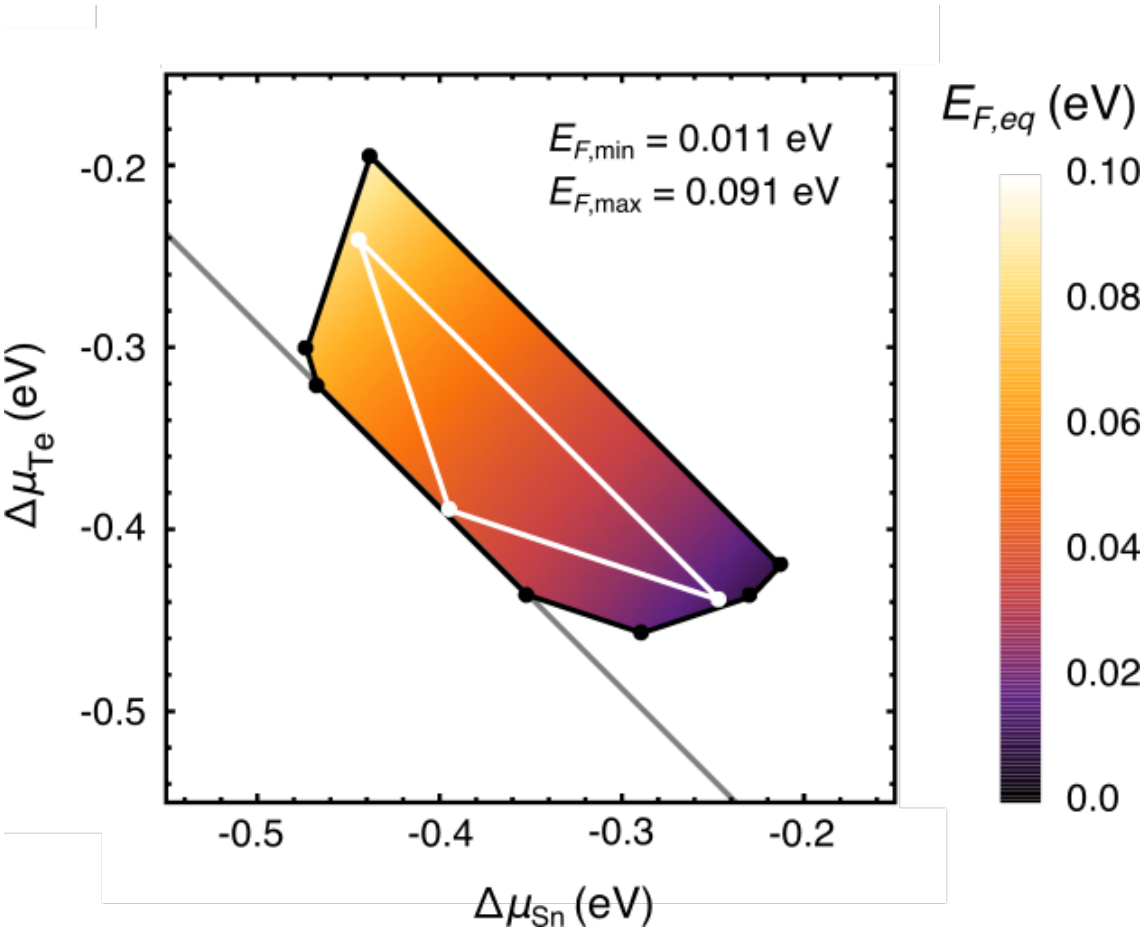

Figure 8: Calculated equilibrium Fermi energy for pre-adjusted chemical potential coordinates. Adjusted shape is seen overlaid in white.